

CONTENTS

	Page
Acknowledgement	c
Abstract in Thai	d
Abstract in English	f
Contents	h
List of Tables	k
List of Figures	l
List of Abreviations and Symbols	w
Chapter 1 Introduction	1
1.1 Background	1
1.2 Principles and Theory	2
1.2.1 Basic AVO Theory	2
1.2.2 AVO Classes Classification	3
1.2.3 Elastic Impedance Inversion	4
1.3 Objective	5
1.4 Methodology	6
Chapter 2 Geologic Background	8
2.1 Introduction	8
2.2 Regional Tectonic Setting	9
2.3 Structural and Stratigraphic Development	11
2.4 Petroleum System	15
Chapter 3 Data Quality Control and Enhancement	17
3.1 Introduction	17
3.2 Well Log Quality Control, Editing and Repairing	17

3.2.1	Well Log Quality Control, Editing	18
a)	Cross plot between depth and velocities	19
b)	Cross plots between density and velocities	20
c)	Cross plots between P-wave velocities and S-wave velocities	23
3.2.2	Well Log Repairing	24
3.3	Seismic Data Enhancement	33
3.3.1	Mute	35
3.3.2	Super Gather	36
3.3.3	Angle Gather	38
3.3.4	Cdp Stack	40
Chapter 4	Well Log Analysis and Seismic Interpretation	42
4.1	Introduction	42
4.2	Well Log Analysis and Interpretation	43
4.2.1	Gamma Ray Log	44
4.2.2	Density Log	45
4.2.3	P-wave Velocity	45
4.2.4	S-wave Velocity	46
4.2.5	Neutron Porosity Log	47
4.2.6	Resistivity Log	48
4.3	Generate Other Logs and Interpretations	49
4.3.1	Vp/Vs Ratio	49
4.3.2	Poisson's ratio	51
4.3.3	Shale Volume (Vsh)	55
4.3.4	Porosity from Density and Neutron	55
4.3.5	Water Saturation (Sw)	57
4.4	Time – Depth Conversion	58
4.5	Seismic Interpretation	63
4.5.1	Horizons Interpretation	64
4.5.2	Faults Interpretation	66
4.5.3	Seismic Amplitude Attributes	69

4.6 Time Structure Map	73
Chapter 5 AVO Modeling	78
5.1 Angle Stack Generation	78
5.2 Well to Seismic Tie	80
5.3 Fluid Replacement Modeling (FRM)	90
5.4 AVO Gradient Analysis	93
5.5 AVO Synthetic Models	95
Chapter 6 Inversion of Seismic Data	103
6.1 Introduction	103
6.2 Elastic Impedance Log Generation	104
6.3 Elastic Impedance Inversion	107
Chapter 7 Discussion and Conclusion	125
7.1 Discussion	125
7.2 Conclusion	136
References	137
Appendices	141
Appendix A	141
Appendix B	141
Curriculum Vitae	143

ลิขสิทธิ์มหาวิทยาลัยเชียงใหม่
Copyright© by Chiang Mai University
All rights reserved

LIST OF TABLES

		Page
Table 2.1	List of formation tops of Well A.	15
Table 3.1	Casing point from final well report.	25
Table 3.2	Comparison between V_s - V_p localized model and Greenberg and Castagna relation for UMA15 interval.	29
Table 3.3	Comparison between V_s - V_p localized model and Greenberg and Castagna relation for MMF10 interval.	30
Table 3.4	Comparison between V_s - V_p localized model and Greenberg and Castagna relation for MMF30 interval.	32
Table 4.1	Seven horizons were picked on seismic data.	64
Table A.1	Different types of well logs in the dataset with their abbreviations and units.	142
Table B.1	VSP data of Well A.	143

LIST OF FIGURES

		Page
Figure 1.1	Intercept versus Gradient crossplot.	3
Figure 1.2	AVO classification scheme	4
Figure 1.3	Main workflow.	7
Figure 2.1	Location of major sedimentary basins within SE Asia. The red block highlights location of the Nam Con Son Basin.	9
Figure 2.2	Tectonostratigraphic of Nam Con Son Basin.	10
Figure 2.3	Example of a seismic section crossing the Nam Con Son Basin.	11
Figure 2.4	Chronostratigraphic diagram of the Nam Con Son Basin.	12
Figure 3.1	Basic well logs editing workflow.	18
Figure 3.2	Depth and Vp cross plot. Red dashed lines zones indicate reservoir intervals.	19
Figure 3.3	Depth and Vs cross plot. Red dashed lines zones indicate reservoir intervals. Yellow box indicates missing value data.	20
Figure 3.4	Density and Vp cross plot. The color lines represent rock physics relationships between Density and P-wave velocity found by Gardner et al., (1974).	21
Figure 3.5	Density and Vs cross plot. The Han Dual Input linear line represents rock physics relationship between density (porosity) and S-wave velocity.	22
Figure 3.6	Vp and Vs cross plot with the Greenberg and Castagna Vp - Vs relations.	24

Figure 3.7	Main logs curves for reservoir characterization. Blue dashed box indicates missing data in S-wave sonic log. Formation tops T65, top and base of two sand bodies MMF10 and MMF15 are in the left hand track.	25
Figure 3.8	Cross plot Vs and Vp for UMA15. Linear relationship between Vs and Vp is defined by equation $V_s = 0.79 * V_p - 485.253$.	27
Figure 3.9	Cross plot Vs and Vp for MMF10. Linear relationship between Vs and Vp is defined by equation $V_s = 0.68 * V_p - 548.775$.	27
Figure 3.10	Cross plot Vs and Vp for MMF30. Linear relationship between Vs and Vp is defined by equation $V_s = 0.58 * V_p - 60.5711$.	28
Figure 3.11	Plot of regression analysis for Vs prediction in UMA15 interval. Track 10 shows the recorded Vs in red and localized predicted Vs in blue while track 14 shows the recorded Vs in red and Greenberg and Castagna relation predicted Vs in blue.	29
Figure 3.12	Plot of regression analysis for Vs prediction in MMF10 interval. Track 10 shows the recorded Vs in red and localized predicted Vs in blue while track 14 shows the recorded Vs in red and Greenberg and Castagna's relation predicted Vs in blue.	30
Figure 3.13	Plot of regression analysis for Vs prediction in MMF30 interval. Track 10 shows the recorded Vs in red and localized predicted Vs in blue while track 14 shows the recorded Vs in red and Greenberg and Castagna's relation predicted Vs in blue.	31
Figure 3.14	Plot of logs for well A. Track 4 shows the recorded Vs in red while track 5 shows the Vs after correction.	32
Figure 3.15	Inline and Cross-line parameters from header of seismic volume.	33
Figure 3.16	Processing history of seismic volume.	34
Figure 3.17	3D migrated seismic gathers.	34
Figure 3.18	Seismic offset gathers after applying mute.	36

Figure 3.19	Before and after creating seismic super gathers. Red dashed lines represent examples of zones where effects of noise are reduced.	37
Figure 3.20	Super gathers at well location from zone of interest.	38
Figure 3.21	The incident angles are displayed on super gather plot.	39
Figure 3.22	Angle gather (40 degrees) at the interest interval.	40
Figure 3.23	CDP super gather stack shows zone of interest. Two oval dashed blue lines show two reservoir intervals UMA15 and MMF30.	41
Figure 4.1	Base map of the study area. Inlines are represented by red color while crosslines are represented by blue color.	42
Figure 4.2	Available logs from Well A (from left to right: GR, Density, P-wave velocity, S-wave velocity, Resistivity, Neutron porosity). The red squares indicate potential reservoir intervals.	44
Figure 4.3	Cross plot of V_p vs V_s of Well A from 2897.27 m to 3750 m. The black arrow indicates the increasing of porosity, clay and pore pressure perpendicular with the saturation trend. The red rectangular represents the gas effect in the reservoir intervals.	47
Figure 4.4	Plot between the Density Log in blue and the Neutron Porosity Log in red color in the interest zone.	48
Figure 4.5	Cross plot of V_p/V_s ratio and S-wave velocity of Well A. The red oval zone represents reservoir intervals.	50
Figure 4.6	Cross section for V_p/V_s and S-wave velocity cross plot.	51
Figure 4.7	Cross plot of Poisson's ratio and V_p/V_s ratio. The red square polygon represents gas sand zone in the cross section.	52
Figure 4.8	Cross plot of Poisson's ratio and P-wave velocity. The red rectangular polygon represents gas sand zone in the cross section.	53
Figure 4.9	Result of well logs interpretation for Well A.	54

Figure 4.10	The zoom out results for reservoir interval UMA15.	54
Figure 4.11	The zoom out results for reservoir interval MMF30.	55
Figure 4.12	Log (depth – time) calibration using linear trends as drift function: track 1, black – Input T-D curve from sonic log, red – calibrated T-D curve; track 2, blue – drift curve fitted to the data using linear segments with knee points; track 3, black – original P-wave sonic log, red – calibrated P-wave sonic log.	60
Figure 4.13	Plot of average velocity between different type of check shot correction.	61
Figure 4.14	Plot of interval velocity between different type of check shot correction.	62
Figure 4.15	Well A before and after checkshots correction.	63
Figure 4.16	Crossline 4918 cross the Well A. Seven horizons were picked on seismic data.	65
Figure 4.17	Inline 1662 cross the Well A. Seven horizons were picked on seismic data.	66
Figure 4.18	Variance attribute at time slice 2980 ms. Cross line 4918 through the Well A shows the horizons and faults represented in the time slice 2980 ms.	67
Figure 4.19	Variance attribute at time slice 2980 ms. Cross line 4718 shows the horizons and faults represented in the time slice 2980 ms.	68
Figure 4.20	Variance attribute at time slice 2980 ms. Inline 1742 shows the horizons and faults represented in the time slice 2980 ms.	68
Figure 4.21	RMS Amplitude from near-angle stack volume along UMA15.	70
Figure 4.22	RMS Amplitude from mid-angle stack volume along UMA15.	71
Figure 4.23	RMS Amplitude from far-angle stack volume along UMA15.	71
Figure 4.24	RMS Amplitude from near-angle stack volume along MMF30.	72
Figure 4.25	RMS Amplitude from mid-angle stack volume along MMF30.	72
Figure 4.26	RMS Amplitude from far-angle stack volume along MMF30.	73
Figure 4.27	Time structure map for horizon T10 (top Oligocene).	74

Figure 4.28	Time structure map for horizon T30.	75
Figure 4.29	Time structure map for horizon Top MMF30.	75
Figure 4.30	Time structure map for horizon T65.	76
Figure 4.31	Time structure map for horizon Top UMA15.	76
Figure 4.32	Time structure map for horizon T85.	77
Figure 4.33	Time structure map for horizon T90.	77
Figure 5.1	Near, mid and far angle gathers (from left to right) at the Well A location.	79
Figure 5.2	Near, mid and far angle stacked volumes (from left to right) at the Well A location with picked horizons.	80
Figure 5.3	Procedure of wavelet estimation.	82
Figure 5.4	Statistical wavelets extracted from seismic data, (a) from full stack, (b) from near angle stack, (c) from mid angle stack, (d) from far angle stack.	83
Figure 5.5	Synthetic tie with full stack using statistical wavelet for well A before and after time shift. The red square indicates the reservoir intervals. The blue traces represent the synthetic while the red traces represent the real seismic data at the well location. The wavelets in the right hand side indicate the cross correlation (CC) between synthetics and real seismic trace. CC increase from -0.195 to 0.679 after time shift of 11 ms down.	84
Figure 5.6	Synthetic tie with near stack using statistical wavelet for well A before and after time shift. The red square indicates the reservoir intervals. The blue traces represent the synthetic while the red traces represent the real seismic data at the well location. The wavelets in the right hand side indicate the cross correlation (CC) between synthetics and real seismic trace. CC increase from -0.084 to 0.735 after time shift of 10 ms down.	84

- Figure 5.7 Synthetic tie with mid stack using statistical wavelet for well A before and after time shift. The red square indicates the reservoir intervals. The blue traces represent the synthetic while the red traces represent the real seismic data at the well location. The wavelets in the right hand side indicate the cross correlation (CC) between synthetics and real seismic trace. CC increase from 0.104 to 0.687 after time shift of 9 ms down. 85
- Figure 5.8 Synthetic tie with far stack using statistical wavelet for well A before and after time shift. The red square indicates the reservoir intervals. The blue traces represent the synthetic while the red traces represent the real seismic data at the well location. The wavelets in the right hand side indicate the cross correlation (CC) between synthetics and real seismic trace. CC increase from 0.444 to 0.576 after time shift of 5 ms down. 86
- Figure 5.9 Phase rotation of wavelet for well to full stack correlation using statistical wavelet. Cross correlation after phase rotation increases from 0.679 to 0.689. The wavelet phase rotation parameter shows -20 degrees. 87
- Figure 5.10 Phase rotation of wavelet for well to near angle stack correlation using statistical wavelet. Cross correlation after phase rotation increases from 0.735 to 0.741. The wavelet phase rotation parameter shows -22 degrees. 87
- Figure 5.11 Phase rotation of wavelet for well to mid angle stack correlation using statistical wavelet. Cross correlation after phase rotation is increases from 0.687 to 0.689. The wavelet phase rotation parameter shows -11 degrees. 88
- Figure 5.12 Phase rotation of wavelet for well to far angle stack correlation using statistical wavelet. Cross correlation after phase rotation remains constant at 0.576. The wavelet phase rotation parameter shows 9 degrees. 88

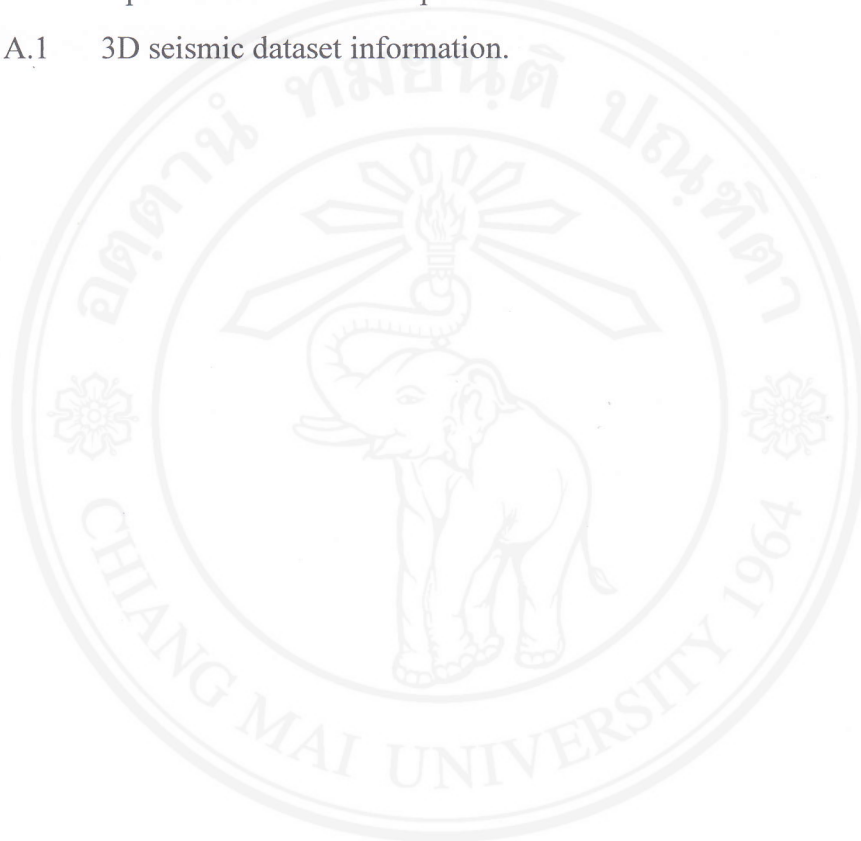
Figure 5.13	Estimated wavelets of seismic data. (a) from well to full stack tie, (b) from well to near angle stack, (c) from well to mid angle stack tie, (d) from well to far angle stack tie.	89
Figure 5.14	Wavelets extracted using well and seismic data. (a) from full stack, (b) from near angle stacks, (c) from mid angle stack, (d) from far angle stack.	90
Figure 5.15	In-situ gas (red curve) is replaced by brine (blue curve) for UMA15 in the Well A. (From left to right) Gamma ray, P-wave velocity, S-wave velocity and Density.	92
Figure 5.16	In-situ gas (red curve) is replaced by brine (blue curve) for MMF30 in the Well A. (From left to right) Gamma ray, P-wave velocity, S-wave velocity and Density.	92
Figure 5.17	Intercept/Gradient analysis for UMA15. (from left to right) Full angle gathers seismic data at the Well A location with picked horizons, Intercept/Gradient curves, Intercept/Gradient cross plot. The red line represents the top of the reservoir while the green line represents the base of the reservoir.	94
Figure 5.18	Intercept/Gradient analysis for UMA15. (from left to right) Full angle gathers seismic data at the Well A location with picked horizons, Intercept/Gradient curves, Intercept/Gradient cross plot. The red line represents the top of the reservoir while the green line represents the base of the reservoir.	95
Figure 5.19	AVO synthetic model for the UMA15 reservoir. (from left to right) Gamma Ray, P-wave velocity, S-wave velocity, Density, Acoustic impedance, AVO synthetic of 100%, in-situ, 100% gas and full angle gather.	99
Figure 5.20	Zoom out of AVO synthetic model for the UMA15 reservoir. (from left to right) Gamma Ray, P-wave velocity, S-wave velocity, Density, Acoustic impedance, AVO synthetic of 100% water, in-situ, 100% gas and full angle gather.	100

Figure 5.21	AVO synthetic model for the MMF30 reservoir. (from left to right) Gamma Ray, P-wave velocity, S-wave velocity, Density, Acoustic impedance, AVO synthetic of 100% water, in-situ, 100% gas and full angle gather.	101
Figure 5.22	Zoom out of AVO synthetic model for the MMF30 reservoir. (from left to right) Gamma Ray, P-wave velocity, S-wave velocity, Density, Acoustic impedance, AVO synthetic of 100% water, in-situ, 100% gas and full angle gather.	102
Figure 6.1	Near, mid and far elastic impedance logs. (from left to right) Gamma Ray, Density, P-wave velocity, S-wave velocity, EI_near, EI_mid and EI_far.	105
Figure 6.2	Plot of EI_near (in yellow), EI_mid (in blue) and EI_far (in red) curve on the same track. The red rectangle represents the UMA15 reservoir interval and the blue rectangle represents the MMF30 reservoir interval.	106
Figure 6.3	Plot of scaled EI_far curve (in blue) with AI curve (in red). The red rectangle represents the UMA15 reservoir interval and the blue rectangle represents the MMF30 reservoir interval.	107
Figure 6.4	Elastic Impedance inversion workflow.	108
Figure 6.5	Cross plot of EI_near versus EI_mid for UMA15 reservoir. The blue polygons represents normal AVO trend while the red polygons represents AVO anomalies trend. The cross section through the well is in the small figure in the right hand side.	109
Figure 6.6	Cross plot of EI_near versus EI_far for UMA15 reservoir. The blue polygons represents normal AVO trend while the red polygons represents AVO anomalies trend. The cross section through the well is in the small figure in the right hand side.	110

Figure 6.7	Cross plot of EI_mid versus EI_far for UMA15 reservoir. The blue polygons represents normal AVO trend while the red polygons represents AVO anomalies trend. The cross section through the well is in the small figure in the right hand side.	110
Figure 6.8	Cross plot of EI_near versus EI_mid for MMF30 reservoir. The blue polygons represents normal AVO trend while the red polygons represents AVO anomalies trend. The cross section through the well is in the small figure in the right hand side.	111
Figure 6.9	Cross plot of EI_near versus EI_far for MMF30 reservoir. The blue polygons represents normal AVO trend while the red polygons represents AVO anomalies trend. The cross section through the well is in the small figure in the right hand side.	112
Figure 6.10	Cross plot of EI_mid versus EI_far for MMF30 reservoir. The blue polygons represents normal AVO trend while the red polygons represents AVO anomalies trend. The cross section through the well is in the small figure in the right hand side.	112
Figure 6.11	Amplitude spectrum of near, mid and far angle stacks from 2450 to 3000 ms (zone of interest) and applied filters for each angle stacks initial model.	114
Figure 6.12	Initial strata model for near angle stack (Xline 4918).	114
Figure 6.13	Initial strata model for mid angle stack (Xline 4918).	115
Figure 6.14	Initial strata model for far angle stack (Xline 4918).	115
Figure 6.15	Inverted near angle stack volumes (Xline 4918).	117
Figure 6.16	Inverted mid angle stack volumes (Xline 4918).	117
Figure 6.17	Inverted far angle stack volume (Xline 4918).	118
Figure 6.18	Inverted near angle stack volume (Inline 1662).	118
Figure 6.19	Inverted mid angle stack volume (Inline 1662).	119
Figure 6.20	Inverted far angle stack volume (Inline 1662).	119

Figure 6.21	Comparison of three elastic impedance volumes at the well A location (Xline 4918). (from left to right) near, mid and far inverted seismic volume.	120
Figure 6.22	Plot of EI_far log at 33 degrees versus inverted seismic EI_far volume in two main reservoirs UMA15 and MMF30 in the well A.	121
Figure 6.23	Cross section and cross plot of Inverted EI_near and Inverted EI_far for the UMA15 reservoir. Note that the cross plot blue and red polygons have already defined from cross plots of EI_near log and EI_far log.	122
Figure 6.24	Cross section and cross plot of Inverted EI_near and Inverted EI_far for the MMF30 reservoir. Note that the cross plot blue and red polygons have already defined from cross plots of EI_near log and EI_far log.	123
Figure 6.25	Map of potential hydrocarbon distribution along horizon UMA15.	124
Figure 6.26	Map of potential hydrocarbon distribution along horizon MMF30.	124
Figure 7.1	Cross plot of AI versus EI_far for the Well A.	128
Figure 7.2	Elastic impedance map through horizon Top UMA15 of inverted near angle stack volume. The black dashed lines represent low elastic impedance zones.	130
Figure 7.3	Elastic impedance map through horizon Top UMA15 of inverted mid angle stack volume. The black dashed lines represent low elastic impedance zones.	131
Figure 7.4	Elastic impedance map through horizon Top UMA15 of inverted far angle stack volume. The black dashed lines represent low elastic impedance zones.	132
Figure 7.5	Elastic impedance map through horizon Top MMF30 of inverted near angle stack volume.	133

- Figure 7.6 Elastic impedance map through horizon Top MMF30 of 134
inverted mid angle stack volume. The black dashed line
represents low elastic impedance zone.
- Figure 7.7 Elastic impedance map through horizon Top MMF30 of 135
inverted far angle stack volume. The black dashed line
represents low elastic impedance zone.
- Figure A.1 3D seismic dataset information. 141



ลิขสิทธิ์มหาวิทยาลัยเชียงใหม่
Copyright© by Chiang Mai University
All rights reserved

LIST OF ABBREVIATIONS AND SYMBOLS

2D	Two dimension
3D	Three dimension
E	East
Hz	Hertz
km	Kilometers
km ²	Square Kilometers
Ma	Million years
m	Meters
ms	milliseconds
N	North
NE	Northeast
NW	Northwest
PSTM	Pre-stack time migration
QC	Quality control
S	South
SE	Southeast
SW	Southwest
W	West

ลิขสิทธิ์มหาวิทยาลัยเชียงใหม่
Copyright© by Chiang Mai University
All rights reserved